Structure factor of fluctuating interfaces: From liquid surfaces to suspended graphene

Jose Hernández-Muñoz,[1] Pedro Tarazona,[2,*] Rafael Ramírez,[3] Carlos P. Herrero,[3] and Enrique Chacón[3]

[1]*Departamento de Física Teórica de la Materia Condensada, IFIMAC Condensed Matter Physics Center, Universidad Autonoma de Madrid, Madrid 28049, Spain*

[2]*Departamento de Física Teórica de la Materia Condensada, IFIMAC Condensed Matter Physics Center, Instituto Nicolás Cabrera de Ciencia de Materiales, Universidad Autonoma de Madrid, Madrid 28049, Spain*

[3]*Instituto de Ciencia de Materiales de Madrid, Consejo Superior de Investigaciones Cientificas, Madrid 28049, Spain*

(Received 13 September 2019; published 21 November 2019)

We obtain the density-density correlation structure in molecular dynamics (MD) simulations of graphene, and analyze it within the capillary wave theory (CWT), developed for fluid surfaces, to describe the thermal corrugations of the graphene sheet with a wave-vector-dependent surface tension $\gamma(q_x)$. The density correlation function (from the atomic positions) is compared with the theoretical prediction by Bedeaux and Weeks (BW), within the CWT, in terms of $\gamma(q_x)$ and the density profile. The agreement is very good, even for relatively large $q_x \approx 0.2$ Å^{-1}, and with very little role for the correlation background, which sets an important difficulty for liquid surfaces. We present and test a generic prediction for the structure factor $S(q_x, q_z)$ from $\gamma(q_x)$, that contains and goes beyond the classical asymptotic expression, developed by Sinha, for the analysis of x-ray surface scattering. We compare our prediction with the formula used in the interpretation of experimental data, that assumes a direct relationship between $\gamma(q_x)$ and the correlation structure for the same wave vector q_x. That relation is exact only for the first (Wertheim's) term of the BW series, and we use our results to test the accuracy of the function $\gamma(q_x)$ estimated through that method.

DOI: 10.1103/PhysRevB.100.195424

I. INTRODUCTION

Surface diffraction techniques, with x rays and neutrons, give experimental access to the thermal corrugations of liquid surfaces through their effects in the density correlation (see, e.g., Refs. [1–4] and references therein). Flexible two-dimensional (2D) structures, like graphene or lipid bilayer membranes, have shape fluctuations similar to those of fluid surfaces, and the analysis of their structure factor also faces the diverging amplitude of long wavelengths corrugations [5–7]. The CWT [8–10] studies the fluctuations of liquid surfaces with a mesoscopic Hamiltonian $\mathcal{H}[\xi]$, a functional of the *intrinsic surface* (IS) that represents the instantaneous shape of the interface in terms of its Fourier components up to an *upper cutoff* wave vector q_u,

$$z = \xi(\vec{x}; q_u) = \sum_{0<|\vec{q}_x|\leqslant q_u} \xi_{q_x} e^{i\vec{q}_x\cdot\vec{x}}, \tag{1}$$

where we take the z axis normal to the mean surface plane with $\vec{x} = (x, y)$ and $\vec{q}_x = (q_x, q_y)$. The mean value $\langle\xi(\vec{x})\rangle = 0$ is fixed as z origin. The CWT assumes independent Gaussian fluctuations of each IS Fourier component, i.e., a quadratic form for the surface Hamiltonian

$$\mathcal{H}[\xi] = \frac{A_0}{2} \sum_{0<|\vec{q}_x|\leqslant q_u} q_x^2 \gamma(q_x) |\xi_{q_x}|^2, \tag{2}$$

where $A_0 \equiv L^2$ is the area of the (flat) mean surface. The mean square values $\langle|\xi_{q_x}|^2\rangle$, at temperature $kT = \beta^{-1}$, give the wave-vector-dependent surface tension,

$$\gamma(q_x) \equiv \frac{kT}{\langle|\xi_{q_x}|^2\rangle q_x^2 A_0} = \gamma_0 + \kappa q_x^2 + \ldots \tag{3}$$

with the macroscopic value γ_0, the surface bending modulus κ, and possibly higher order terms.

The density profile $\rho(z) = \langle\varrho(\vec{r})\rangle$ is the statistical average of the density operator $\varrho(\vec{r}) = \sum_{i=1,N} \delta(\vec{r} - \vec{r}_i)$ for the instantaneous atomic positions. The CWT splits the average as $\langle\ldots\rangle = \langle\langle\ldots\rangle_{\{\vec{r}\}\in\xi}\rangle_\xi$, with the inner average over the states compatible with an IS shape, and the mesoscopic average $\langle\ldots\rangle_\xi$ over the function $\xi(\vec{x})$, through the Hamiltonian (2). The *upper cutoff* q_u in (1) is the (main) control parameter for the splitting of the thermal average and, by taking q_u not too high, the CWT assumes that the surface fluctuation effects on the density profile $\rho(z)$ may be described as an *intrinsic profile* $\rho^{\rm in}(z; q_u)$ shifted to follow the IS fluctuations

$$\rho(z) \simeq \langle\rho^{\rm in}(z - \xi(\vec{x}); q_u)\rangle_\xi = \int d\xi\ \rho^{\rm in}(z - \xi; q_u) P(\xi). \tag{4}$$

The average $\langle\ldots\rangle_\xi$, through the probability distribution $P(\xi)$ for the local IS position, smooths $\rho(z)$ as L increases and, associated to that effect, the density correlation $G(x_{12}, z_1, z_2) = \langle\varrho(\vec{r}_1)\varrho(\vec{r}_2)\rangle - \rho(z_1)\rho(z_2)$ develops a logarithmic tail for large $x_{12} = |\vec{x}_1 - \vec{x}_2|$. The transverse Fourier transform $G(z_1, z_2; q_x)$ has a term

$$G^{\rm W}(z_1, z_2, q_x) = \frac{\rho'(z_1)\rho'(z_2)}{\beta\gamma(q_x)q_x^2}, \tag{5}$$

*pedro.tarazona@uam.es

that diverges for $q_x = 0$, proportionally to the derivative with respect to z of the mean density profile, $\rho'(z) = d\rho(z)/dz$. The prediction of this term by Wertheim [11] (originally in terms of γ_0) was later followed by the work of Bedeaux and Weeks (BW) [12] that extended the contribution of the IS fluctuations beyond (5), to show the divergence of the surface structure factor as

$$S(q_x, q_z) = \int dz_1 dz_2\, G(z_1, z_2, q_x)\, e^{iq_z(z_1 - z_2)} \propto \frac{|\Phi(q_z)|^2}{q_x^{2-\eta}} + \text{regular terms}, \tag{6}$$

with $\eta = q_z^2/(2\pi\beta\gamma_0)$ in the exponent and the surface density structure in

$$\Phi(q_z) = \int dz\, \rho'(z)\, e^{iq_z z}. \tag{7}$$

Attempts to use (5-6) to obtain $\gamma(q_x)$ from x-ray diffraction experiments [2,3,13,14], computer simulations [4,15,16], and DF theories [4,17–22] have been puzzling, with very different predictions for $\gamma(q_x)$ except for the limit $\gamma(0) = \gamma_0$.

The aim of this work is to use molecular dynamics (MD) simulations of a realistic model of graphene to get directly $\gamma(q_x)$ from the shape corrugations, and to check whether and how it could be reconstructed from the results for $G(z_1, z_2, q_x)$ (accessible to computer simulations) and from $S(q_x, q_z)$ (accessible to diffraction experiments). Besides its inherent interest, graphene provides an ideal case of fluctuating surface, since its 2D atomic structure dodges the most difficult steps in the matching of the atomistic (MD) and the mesoscopic (CWT) views. Moreover, even for low q_x a liquid surface has a background of fluctuations modes G_b not related to the IS corrugations. This background includes any on-plane fluctuation of the atomic positions, as well as any effect of the atomic vibrations in the z direction that (for large q) might escape from the CWT assumption of independent Gaussian fluctuations for the IS Fourier components ξ_{q_x}. It is only the difference $\Delta G \equiv G - G_b$ that gives the bare contribution of the IS fluctuations, from which we may hope to extract $\gamma(q_x)$. The regular and stiff 2D lattice of a graphene sheet makes $G_b \ll G$ even for relatively large q_x, so that the full G may be used for a quantitative comparison with the CWT predictions. On the other hand, the theoretical analysis of $S(q_x, q_z)$ for a liquid-vapor interface is easier in the strict grazing incidence condition [1,4] $q_z = 0$. However, a (small) $q_z > 0$ is unavoidable under practical experimental conditions for the grazing-incidence small-angle x-ray scattering (GISAXS) technique [13,14,23]. For any 2D system like graphene, the lack of density contrast between the two sides of the IS cancels out the whole contribution of the IS fluctuations to $S(q_x, q_z)$ for $q_z = 0$, so that the analysis for $q_z > 0$ becomes compulsory.

Section II presents the essentials of the analysis by Bedeaux and Weeks (BW) [12], and its equivalence with the analysis of the Debye-Waller factor in 2D crystals [5] for the $q_x = 0$ diffraction peak. Section III presents the MD simulations of a graphene model and the direct results for $\gamma(q_x)$ from the mean square values $\langle|\xi_{q_x}|^2\rangle$. Section IV compares the MD results for $G(z_1, z_2, q_x)$ with the BW prediction, to show that is rather accurate, but only when we consider the full series of which (5) is just the first ($n = 1$) term. The small correlation background makes graphene a good choice to try and get experimental access to $\gamma(q_x)$ from surface diffraction techniques. To that effect, we analyze in Sec. V the signature of $\gamma(q_x)$ in $S(q_x, q_z)$, beyond the strict grazing incidence condition $q_z = 0$. The analysis of the transverse size shows the converge from the periodic MD boxes to the sampled areas in diffraction experiments, much larger and without periodic boundary conditions. In the continuous limit for the $\vec{q}_x$ sums, we present a generic expression for $S(q_x, q_z)$ that recovers the analytical prediction by Sinha [5] (6) as the leading term at low q_x. We get also the correction that reflects the short-ranged structure of the IS fluctuations and that contains the effects of the function $\gamma(q_x)$ beyond its γ_0 limit. The role of the mean and the intrinsic density profiles to determine the prefactor in (6) is clarified. In Sec. VI, we compare the different proposals to obtain $\gamma(q_x)$ from $G(z_1, z_2, q_x)$ (in computer simulations and theoretical density functional analysis) and from experimental $S(q_x, q_z)$ data. We conclude with the general implications for the interpretation of surface diffraction experiments in terms of $\gamma(q_x)$.

II. SURFACE CORRELATION STRUCTURE AND BEDEAUX-WEEKS SERIES

In 1985 Bedeaux and Weeks [12] (BW), working within the CWT assumption of Gaussian probability for the IS Fourier components, showed that (5) is just the $n = 1$ term of a series that gives the contribution from the IS fluctuations to the density correlation as

$$G^{\mathrm{BW}}(z_1, z_2, q_x) = \sum_{n=1}^{\infty} \frac{\hat{\mathcal{S}}_n(q_x)}{n!} \frac{d^n\rho(z_1)}{dz_1^n} \frac{d^n\rho(z_2)}{dz_2^n}, \tag{8}$$

with derivatives of $\rho(z)$ at any order, and where

$$\hat{\mathcal{S}}_n(q_x) \equiv \int d^2\vec{x}\, \mathcal{S}(\vec{x})^n\, e^{i\vec{q}_x\cdot\vec{x}}, \tag{9}$$

is the transverse Fourier transform of the n-power height-height correlation function $\mathcal{S}(x_{12}) = \langle\xi(\vec{x}_1)\xi(\vec{x}_2)\rangle$.

The $n = 1$ term uses the Fourier transform of $\mathcal{S}(x)$

$$\hat{\mathcal{S}}(q_x) \equiv \hat{\mathcal{S}}_1(q_x) = A_0\langle|\xi_{q_x}|^2\rangle = (\beta\gamma(q_x)q_x^2)^{-1}, \tag{10}$$

so that its contribution to $G(z_1, z_2, q_x)$ is (5), determined by the value of $\gamma(q_x)$ at the same transverse vector. The contribution of this term to $S(q_x, q_z)$ is

$$S^{\mathrm{W}}(q_x, q_z) = \int dz_1 dz_2 G^{\mathrm{W}}(z_1, z_2, q_x) e^{iq_z z_{12}} = \frac{|\Phi(q_z)|^2}{\beta\gamma(q_x)q_x^2}, \tag{11}$$

The full BW series may be Fourier transformed as

$$\begin{aligned} S^{\mathrm{BW}}(q_x, q_z) &\equiv \int dz_1 dz_2 G^{\mathrm{BW}}(z_1, z_2, q_x) e^{iq_z z_{12}} \\ &= \sum_{n=1}^{\infty} \frac{q_z^{2(n-1)}|\Phi(q_z)|^2}{n!} \int d^2\vec{x}\mathcal{S}(\vec{x})^n e^{i\vec{q}_x\cdot\vec{x}} \\ &= \frac{|\Phi(q_z)|^2}{q_z^2} \int d^2\vec{x}\left(e^{q_z^2\mathcal{S}(\vec{x})} - 1\right)e^{i\vec{q}_x\cdot\vec{x}}. \end{aligned} \tag{12}$$

This sum of the series makes contact with the usual analysis of the surface structure factor in terms of the two-particle distribution $\rho^{(2)}(\vec{r}_1,\vec{r}_2)$. Following Sinha [5], the contribution from the IS fluctuations is the average $\langle\dots\rangle_\xi$ of two shifted intrinsic density profiles, $\langle\rho^{\rm in}(z_1-\xi(\vec{x}_1))\rho^{\rm in}(z_2-\xi(\vec{x}_2))\rangle_\xi$, leading to

$$\begin{aligned} S(q_x,q_z) &= \int d^2\vec{x}_{12}\, e^{i\vec{q}_x\cdot\vec{x}_{12}}\Big\langle e^{iq_z(\xi(\vec{x}_1)-\xi(\vec{x}_2))} \\ &\quad\times\int dz_1\rho^{\rm in}(z_1-\xi(\vec{x}_1))e^{iq_z(z_1-\xi(\vec{x}_1))} \\ &\quad\times\int dz_2\rho^{\rm in}(z_2-\xi(\vec{x}_2))e^{-iq_z(z_2-\xi(\vec{x}_2))}\Big\rangle_\xi \\ &= \frac{|\Phi^{\rm in}(q_z)|^2}{q_z^2}\int d^2\vec{x}_{12}e^{i\vec{q}_x\cdot\vec{x}_{12}}\langle e^{iq_z(\xi(\vec{x}_1)-\xi(\vec{x}_2))}\rangle_\xi \\ &= \frac{|\Phi(q_z)|^2}{q_z^2}\int d^2\vec{x}\; e^{i\vec{q}_x\cdot\vec{x}}\; e^{q_z^2\mathcal{S}(\vec{x})}. \end{aligned} \tag{13}$$

The Gaussian distribution for each ξ_{q_x}, assumed to get (8), gives here the Debye-Waller factor for the IS fluctuations, $\langle e^{iq_z(\xi(\vec{x}_1)-\xi(\vec{x}_2))}\rangle_\xi = e^{-q_z^2\langle(\xi(\vec{x}_1)-\xi(\vec{x}_2))^2\rangle_\xi/2} = e^{-q_z^2(\mathcal{S}(0)-\mathcal{S}(x_{12}))}$. The $|\Phi(q_z)|^2$ factor in (13) is obtained as $|\Phi^{\rm in}(q_z)|^2e^{-q_z^2\mathcal{S}(0)}$, from the Fourier transform of the derivative of the intrinsic profile,

$$\Phi^{\rm in}(q_z) = \int dz\,\frac{d\rho^{\rm in}(z;q_u)}{dz}\,e^{iq_zz}, \tag{14}$$

assuming the Gaussian convolution in (4) with mean square width $\langle\xi^2\rangle=\mathcal{S}(0)$.

The only difference between (12) and (13) is the -1 term subtracted from $e^{q_z^2\mathcal{S}(x)}$. This term would come as the $n=0$ (missing) term in the BW series (8), i.e. the product $\rho(z_1)\rho(z_2)$ subtracted from $\rho^{(2)}(\vec{r}_1,\vec{r}_2)$ to get the correlation. In $S(q_x,q_z)$ this term gives the specular reflection ray, with a value $A_0|\Phi(q_z)|^2/q_z^2$ for $q_x=0$ and null for any $q_x\neq0$, which gives the Fresnell reflectivity of a flat interface with the density profile $\rho(z)$. Therefore it is clear that $G^{\rm BW}(z_1,z_2,q_x)$ is exactly (under the assumption of Gaussian IS fluctuations) the diffuse scattering by the corrugated surface. Wertheim's term (5) corresponds to the linear expansion of the Debye-Waller factor $e^{q_z^2\mathcal{S}(x)}-1\approx q_z^2\mathcal{S}(x)$ in (13).

In a liquid surface, $q_z=0$ gives $\Phi(0)=\Delta\rho$, the density difference between the two coexisting phases, and cancels all the $n\geqslant2$ terms in the BW series (8). This is the strictest limit of the GISAXS experiments which has been used in the analysis of MD simulations [1,4], to get $\gamma(q_x)$ from $S(q_x,0)$ through the identification of (5) with the diffuse scattering signal. Under practical experimental conditions the strict $q_z=0$ limit is unreachable for liquid surfaces, and it would be useless for graphene, lipid bilayers, or any other 2D system, since there is no difference between the density at two sides and hence $\Phi(0)=0$. Therefore the interpretation of GISAXS data requires to consider the effects of small but not null q_z. Often this has been done assuming that (6) could be generalized to an exponent $\eta(q_x)$ associated to $\gamma(q_x)$ [13,14,23]. We discuss below the validity of that approach.

III. MD-ISM FOR A SUSPENDED GRAPHENE SHEET

We have run classical molecular dynamics (MD) simulations of a suspended graphene sheet using an empirical long-range carbon bond-order potential, the so-called LCBOPII [24,25]. The parametrization is the same as in earlier works [26,27], which yields a realistic description of vibrational, mechanical, and thermal properties [27,28], with a bending constant of 1.48 eV for a single graphene layer a low temperature. We use standard algorithms [29,30] for the isothermal-isobaric ensemble, with $N=8400$ carbon atoms, chains of four Nosé-Hoover thermostats at temperature $T=300$ K, coupled to each atomic coordinate, and the additional chain of four barostats coupled to the in-plane area of the simulation cell, to fix the applied in-plane tensile stress P_x [31]. The results reported here correspond to $P_x=-0.16$ N/m, which gives $L=148.26$ Å as the mean side of the square MD box, and a much higher tensile stress $P_x=-3.2$ N/m that gives $L=149.67$ Å. These values of P_x cover the range of estimates for the experimental stress-strain of suspended graphene [32,33]. The equations of motion have been integrated with the reversible reference system propagator algorithm (RESPA), which allows different time steps for the integration of slow and fast degrees of freedom [34]. The time step Δt corresponding to the interatomic forces is 1 fs, while for the evolution of the fast dynamical variables, including the thermostats, we used a time step $\delta t=\Delta t/4$.

The corrugations of the graphene sheet could be analysed within the language of phonons, as harmonic displacements of the atomic positions from the sites in the periodic 2D lattice, giving the acoustic band of frequencies $\omega_A(q_x)$ with z polarization. Then, the divergence of the structure factor for low q_x appears in the Debye-Waller factor [6,7]. The CWT language, with the thermal fluctuations of a mathematical surface $z=\xi(\vec{x};q_u)$, corresponds to a continuous limit representation of the atomic vibrations. The intrinsic sampling method (ISM) [35–37] was developed to optimize that description over the largest possible range of q_x, in the harder problem of a liquid surface. For a graphene sheet, the task is much easier, since it does not require to choose the atomic positions associated to the interface. As an *ideal interface* all the carbon positions are used as *surface pivots* so that at the maximum resolution the IS is defined as a triangulated surface with the edges joining each carbon atom to its nearest neighbors. We use the periodicity of the simulation box on the x plane to get the Fourier components of that surface by least-square fits, up to a large $|\vec{q}_x|\lesssim0.41$ Å^{-1}, to leave room for the choice of the upper cutoff q_u that defines $z=\xi(\vec{x};q_u)$ as the truncated Fourier series (1).

The sampling of 20 000 configurations, sorted each 500 MD steps, gives the mean square values $\langle|\xi_{q_x}|^2\rangle$ that are used in (3) to get $\gamma(q_x)$, as presented in Fig. 1. For biological membranes and liquid-vapor surfaces the contribution from the bending modulus κ gets entangled with internal fluctuation modes of the interface, but the graphene sheet shows quadratic behavior $\gamma(q_x)\simeq\gamma_0+\kappa q_x^2$ over a large q_x range. We get $\beta\gamma_0=0.66087$ Å^{-2} and $\beta\kappa=63.5669$ for $P_x=-0.16$ N/m, and $\beta\gamma_0=7.8749$ Å^{-2} and $\beta\kappa=62.045$ for the tenser graphene sheet with $P_x=-3.2$ N/m. As a test for the physical significance of this $\gamma(q_x)$ we compare it in

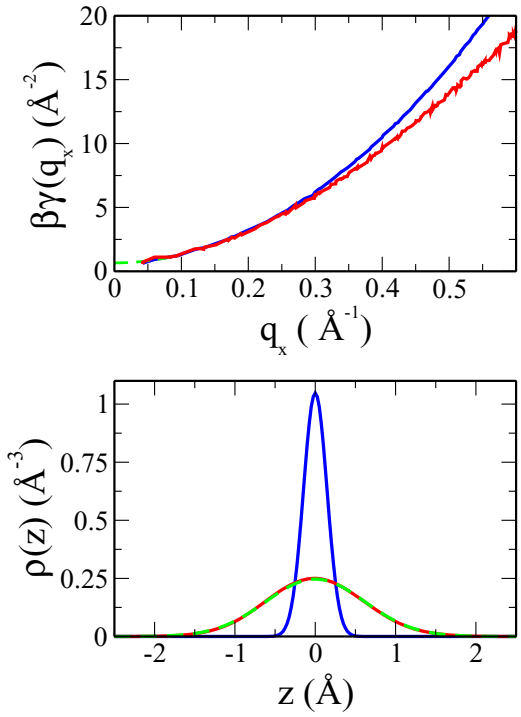

FIG. 1. (Top) Effective wave-vector-dependent surface tension. The blue line is $\gamma(q_x)$ from the mean square amplitude of the fluctuating modes of $\xi(\vec{x})$, in Eq. (3), and the green dashed line is fit to the quadratic form $\gamma(q_x) = \gamma_0 + \kappa q_x^2$ as explained in the text. The red line is the dynamical result Eq. (15), from the dispersion relation of the acoustic vibrational modes. (Bottom) Density profiles. Red full line: the MD mean density profile $\rho(z)$ in the MD box of size $L = 148.24$ Å, blue full line the intrinsic profile $\rho^{in}(z; q_u)$ with $q_u = 0.21$ Å^{-1}, and independent of L. Dashed green line: the mean density profile obtained from the Eq. (4), with the probabiliy distribution $P(\xi)$ along the same MD-ISM used to get $\rho^{\rm in}(z; q_u)$, which is over the direct MD red. Both panels for tensile stress $P_x = -0.16$ N/m.

the top panel of Fig. 1 with the dynamical (dyn) counterpart, described from the frequency band $\omega_A(q_x)$ obtained in the same MD simulations. Assuming a continuous 2D mass density $\rho_{\rm 2D}$, the energy cost of the corrugations should be given by

$$\gamma^{\rm dyn}(q_x) = \rho_{\rm 2D}\omega_{\rm A}^2(q_x)/q_x^2. \tag{15}$$

Good agreement between the dynamical and the ISM thermal fluctuations results for $\gamma(q_x)$ had been reported for liquid surfaces [38]. For graphene the agreement becomes excellent up to much larger q_x, all over the quadratic range of $\gamma(q_x) \simeq \gamma_0 + \kappa q_x^2$. Nevertheless, we have to warn about the low q_x results, for which the continuous approach should be excellent. However, with our lower tensile stress these IS dynamical modes are very slow and a good statistical sampling of $\langle|\xi_{q_x}|^2\rangle$ is only achieved for very long MD simulation times. Small deviations from the quadratic form observed in Fig. 1 at low q_x should be taken as the error bars for the accuracy of our MD results. The probability distribution $P(\xi)$ for the local fluctuations of the IS in (4) is found to be accurately Gaussian, with mean square value

$$\langle|\xi|^2\rangle \equiv \mathcal{S}(0) = \sum_{0<q_x\leqslant q_u} \langle|\xi_{q_x}|^2\rangle. \tag{16}$$

The parameter q_u controls how closely the mathematical surface $z = \xi(\vec{x}; q_u)$ follows the atomic positions, to reach as far as possible with the continuous description, while still keeping the CWT assumptions (4). We have fixed $q_u = 0.21$ Å^{-1} and the intrinsic profile, calculated as the MD-ISM average

$$\rho^{\rm in}(z; q_u) = \langle\varrho(\vec{x}, z + \xi(\vec{x}; q_u))\rangle, \tag{17}$$

forms the narrow peak in Fig. 1, reflecting the small fluctuations in the distance from the atomic positions to the IS. A lower value of q_u would give smoother IS and a broader $\rho^{\rm in}(z; q_u)$, but it would restrict the application of the CWT Hamiltonian (2) to a narrower band $0 < q_x \leqslant q_u$. On the other direction, a higher q_u would give an even narrower peak in $\rho^{\rm in}(z; q_u)$, but it would fail to satisfy the CWT assumption (4). As shown in Fig. 1, with our choice for q_u the convolution of $\rho^{\rm in}(z; q_u)$ and the Gaussian distribution $P(\xi)$ gives mean density profile in excellent agreement with the direct average $\rho(z) = \langle\varrho(\vec{r})\rangle$ along the MD simulations.

Our choice $q_u = 0.21$ Å^{-1} is much lower than the main peak in the structure factor of the graphene sheet at $q \approx 3$ Å^{-1}. This guarantees that the correlation effects for $q_x \leqslant q_u$, described by the BW series (8), are well separated from other vibrational modes. Notice also that this value of q_u is very close to the value of q_x where $\gamma^{\rm dyn}(q_x)$ begins to separate from the structural $\gamma(q_x)$. Liquid surfaces require lower q_u and costly simulations with very large box sizes to get just a few discrete values within the range $q_x \geqslant 2\pi/L$ set by the simulation box. The larger q_u for graphene makes easier to analyze $G(z_1, z_2, q_x)$ over a broad range of wave vectors.

IV. MD RESULTS AND BW SERIES FOR THE DENSITY CORRELATION

For any $\vec{q}_x$ on the reciprocal lattice of the simulation box, the density correlation is obtained from

$$\begin{aligned}\left\langle \frac{1}{A_0}\sum_{i,j=1}^{N} e^{i\vec{q}_x\cdot(\vec{x}_i-\vec{x}_j)}\delta(z_1-z_i)\delta(z_2-z_j)\right\rangle \\ = \rho(z_1)\delta(z_1-z_2) + \rho^{(2)}(z_1, z_2, q_x) \\ = G(z_1, z_2, q_x) + \rho(z_1)\rho(z_2)\delta_{0,q_x},\end{aligned} \tag{18}$$

averaged as a (z_1, z_2) matrix with binning $\Delta z = 0.1$ Å. The statistics was accumulated, with z_1 and z_2 referred to the instantaneous mean plane $z = \xi_0 \equiv 0$. There are two terms that distinguish the total correlation G and the pair distribution $\rho^{(2)}$, one is the $q_x = 0$ contribution $\rho(z_1)\rho(z_2)$ that gives the specular refectivity contribution in $S(0, q_z)$ for a flat interface. The second term, independent of q_x, is the ideal self-correlation from the $i = j$ terms in the double sum over the atomic positions. The bottom row of Fig. 2 presents $G(z_1, z_2, q_x)$, for our system with the lowest tensile stress, excluding the self-correlation term. That term is important in fluid surfaces and bilayer membranes and it has to be taken properly into account as part of G_b, since it is not part of the

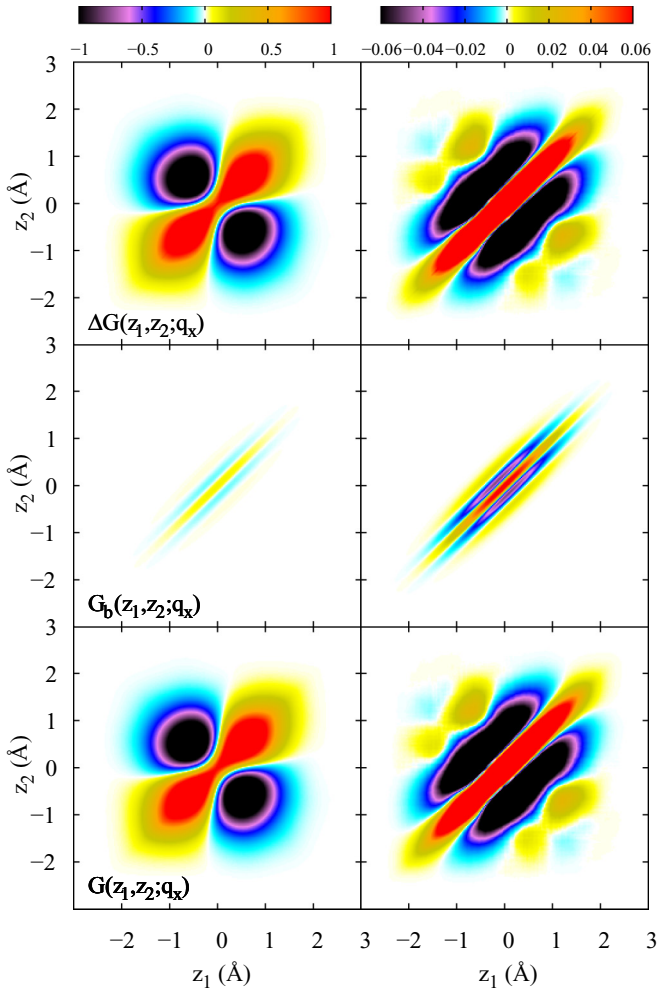

FIG. 2. The density-density correlation functions from MD simulation with tensile stress $P_x = -0.16$ N/m. (Left column) $q_x = 0.042$ Å^{-1} and (right column) $q_x = 0.12$ Å^{-1}. (Bottom row) Total $G(z_1, z_2; q_x)$, Eq. (18). (Middle row) Non-CW background $G_b(z_1, z_2; q_x)$, Eq. (19). (Top row) Bare CW contribution $\Delta G = G - G_b$;

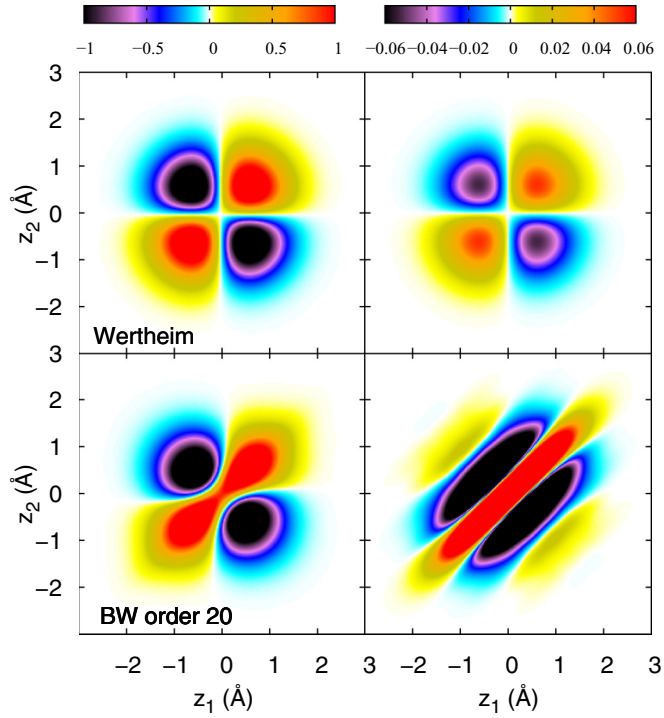

FIG. 3. The Bedeaux-Weeks density-density correlation function with the lateral size L of the MD simulation cell and tensile stress $P_x = -0.16$ N/m. (Left column) $q_x = 0.042$ Å^{-1} and (right column) $q_x = 0.12$ Å^{-1}. (Bottom row) $G^{\rm BW}(z_1, z_2; q_x)$, with the series (8) up to order $n = 20$. (Top row) Wertheim's approximation $G^{\rm W}(z_1, z_2; q_x)$, i.e., the $n = 1$ term of the BW series.

BW series. However, in the case of graphene its contribution is very small. The left column corresponds to the lowest q_x within our simulation box, $q_x = 2\pi/L = 0.042$ Å^{-1}, in the right column is for $q_x = 0.12$ Å^{-1}, three times larger.

The application of the ISM to extract the correlation background G_b was proposed and tested in a recent publication [39]. The main concept is the intrinsic density correlation, $G^{\rm in}(z_1, z_2; q_x)$, obtained changing z_α ($\alpha = i, j$) in (18) by $z_\alpha^{\rm in} \equiv z_\alpha - \xi(\vec{x}_\alpha; q_u)$, to refer the position of the two particles to the IS position above each one. That eliminates the effects of the IS fluctuations and leaves a $G^{\rm in}$ which does not depend on the box size L. In a liquid surface, G_b includes the correlation structure of the dense liquid in the bulk, for z_1 and z_2 far away from the interface. For graphene, this *intrinsic background* contains only the small effects of the corrugations with $q_x > q_u$, which are not included in $\xi(\vec{x}; q_u)$. That reduces $G^{\rm in}$ to a small trace for z_1 and z_2 over the narrow peak of the intrinsic density profile. The actual background correlation G_b is obtained [39] by convolution with the probability distribution $P(\xi)$,

$$G_b(z_1, z_2, q_x) = \int d\xi\, P(\xi)\, G^{\rm in}(z_1 - \xi, z_2 - \xi, q_x). \quad (19)$$

This function, represented in the middle row of Fig. 2, is spread over a larger range of z_1 and z_2, taking the aspect of a narrow diagonal band $|z_1 - z_2| \lesssim 0.5$ Å, in the same way as the intrinsic density profile (4) if spread to give the (L-dependent) mean density profile in Fig. 1. The relative contribution of G_b to the total G in graphene is much lower than for liquid surfaces [39], even at rather high q_x. Therefore, and contrary to what happens in liquid-vapor surfaces, the shape of $\Delta G \equiv G - G_b$ in the top row of Fig. 2 is very similar to the full G in the bottom row. Notice that the ideal-gas self-correlation (i.e., the $i = j$ terms in (18)) is exactly equal in G and G_b so that it is fully eliminated in the bare IS contribution ΔG. That brings us to the first conclusion of this work that the correlation background G_b is almost negligible in graphene. This agrees with the result obtained with dark-field electron microscopy [40] for a monolayer of graphene. Even if T is a factor ten smaller than the Debye temperature, the Debye-Waller factor becomes several times larger than the $T = 0$ result. This conclusion is crucial for the experimental access to $\gamma(q_x)$ from the surface structure factor $S(q_x, q_z)$ in graphene, since we may use the contribution from the IS fluctuations [(12) and (13)] as (nearly) the whole structure factor.

The Bedeaux-Weeks series (8) is the CWT prediction for ΔG. The height-height correlation in real space

$$\mathcal{S}(\vec{x}) = \sum_{0<q_x}^{q_u} \langle |\xi_{q_x}|^2 \rangle e^{i\vec{q}_x\vec{x}} = \sum_{0<q_x}^{q_u} \frac{e^{i\vec{q}_x\vec{x}}}{\beta\gamma(q_x)q_x^2 A_0}, \tag{20}$$

may be calculated directly from the MD-ISM results for $\langle |\xi_{q_x}|^2 \rangle$, within the MD system size. With $\mathcal{S}(\vec{x})$ and $\rho(z)$ we calculate the factors $\hat{\mathcal{S}}_n(q_x)$, to get $G^{\rm BW}(z_1, z_2, q_x)$ in (8). The study of the convergence of the BW series (8) is presented as Ref. [41]. The results presented in the bottom row of Fig. 3 show a great similarity with $G \simeq \Delta G$ (bottom and top rows in Fig. 2), and clear differences with $G^{\rm W}$ (top row Fig. 3), which is the $n = 1$ term of the series. This Wertheim's term (5) exhibits perfect factorization $\rho'(z_1)\rho'(z_2)$ and the $\sim q_x^{-2}$ divergence at low q_x. The factors $\hat{\mathcal{S}}_n(q_x)$ for $n \geqslant 2$ in (8) and (9) have a finite $q_x = 0$ limit, i.e., they do not contribute to the long-range decay of $G(x_{12}, z_1, z_2)$, but still they can give an important contribution. Notice that, contrary to the $n = 1$ case, these $\hat{\mathcal{S}}_n(q_x)$ depend on the system size and they are not q_x-local; i.e., to get their value for a given q_x we need the full $\gamma(q_x)$ function, including its upper limit q_u.

It is clear that Wertheim's term (5) is far from being the full contribution of the IS fluctuations to the density correlation of suspended graphene, the accurate representation of G is only obtained with the full BW series, and the theoretical assumptions leading to that prediction seem to be rather accurate up to large q_x. For the lowest q_x, the practical convergence of the BW series is reached for $n \approx 3$–5. However, for q_x three times larger we have to add up to $n \approx 20$. That tendency follows the results for cold liquid surfaces [39], with structured density profiles, that got important contributions to $G^{\rm BW}$ beyond Wertheim's term. The density profile of graphene is a narrow peak, so we expect a very slow convergence of the series, but we may use the Gaussian fit to the density profile Fig. 1 to get the derivatives of $\rho(z)$, up any high n.

Within the MD-ISM, the definition of $\Delta G \equiv G - G_b$ and its CWT prediction $G^{\rm BW}$ in (8) are linked by the (q_u-controlled) separation between the IS fluctuations and the remaining background. The choice of a lower q_u would still give CWT-consistent results, with a broader $\rho^{\rm in}(z)$ giving the same $\rho(z)$ through the convolution (4) with a narrower $P(\xi)$. But in that case we would transfer some IS fluctuations to be considered as part of the background G_b, rather as part of ΔG, and that may spoil the result $G_b \ll \Delta G \simeq G$ discussed above.

V. THE SURFACE STRUCTURE FACTOR OF SUSPENDED GRAPHENE

We analyze here the results of the previous section but now in terms of the structure factor $S(q_x, q_z)$, which may open the experimental access to $\gamma(q_x)$. Figure 4 shows the results as a function of q_z, for two values of q_x, in the system with tensile strength $P_x = -3.2$ N/m. The left column compares the total $S(q_x, q_z)$, directly from our MD simulation, with $S^{\rm BW}$ from (12), and with Wertheim's term $S^{\rm W}$ from (11). They all agree in the low-q_z limit, taking the form $S \approx (\rho_{\rm 2D} q_z)^2/(\beta\gamma(q_x)q_x^2)$. This parabolic dependence $\sim q_z^2$, at low q_z, is peculiar of 2D systems like graphene, which have $|\Phi(q_z)| \sim \rho_{\rm 2D} q_z$ and hence $|\Phi(0)| = 0$. Liquid surfaces, with a positive $\Phi(0) = \Delta\rho$, have $S(q_x, q_z)$ with a broad maximum at $q_z = 0$ which makes GISAXS the best experimental probe to measure the surface fluctuations in those systems. Thus, for graphene (or other 2D structures), the simplest interpretation of the structure factor as $S^{\rm BW} \simeq S^{\rm W}$ is restricted to the region where $S(q_x, q_z)$ is rather small, and that region shrinks as q_x grows. The maximum signal of the IS fluctuations appears in the region where the theoretical analysis has to go clearly beyond Wertheim's ($n = 1$) term in the BW series.

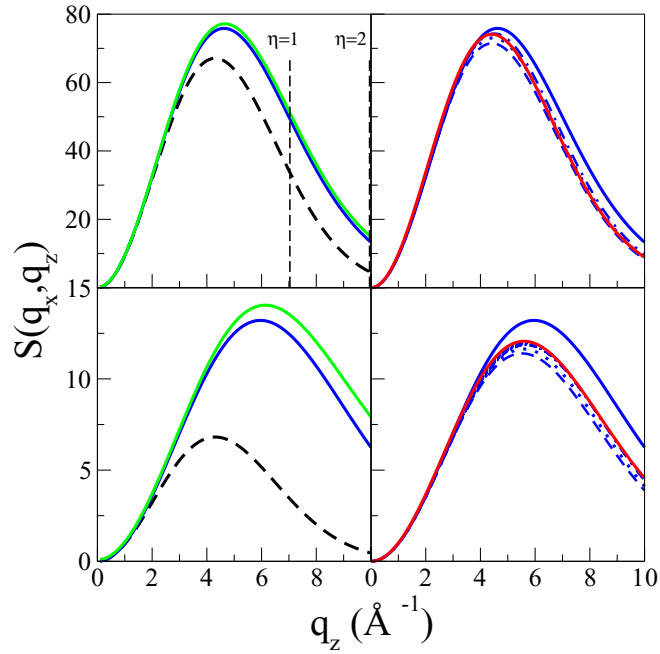

FIG. 4. The structure factor $S(q_x, q_z)$ with tensile stress $P_x = -3.2$ N/m. We show two values of q_x: (top) $q_x = 0.042$ and (bottom) 0.12 Å^{-1}. Left column, with the simulation lateral size $L = L_{\rm MD}$: The green line shows the direct MD result $S(q_x, q_z)$; the blue line $S^{\rm BW}(q_x, q_z)$ (up to order $n = 20$ for convergence), and the black dashed line is Wertheim approximation $S^{\rm W}(q_x, q_z)$. Right column shows the dependence of $S^{\rm BW}(q_x, q_z)$ with the lateral size. The full blue line $S^{\rm BW}$ (as on the left) with $L = L_{\rm MD}$. The results using Eqs. (12) and (20) in larger periodic boxes are: dashed lines $L = 2L_{\rm MD}$, dotted line: $L = 8L_{\rm MD}$ and dashed-dotted line: $L = 32L_{\rm MD}$. The red line is the result of Eq. (21), the continuous limit for very large L, without periodic boundaries.

For the lower q_x (top row in Fig. 4), the BW prediction is very close to the full MD result over the whole range of q_z. For the higher value of q_x (bottom) there is some discrepancy, which quantifies the small visual differences between the bottom-right panels in Figs. 2 and 3. The main possible source for the discrepancies are small deviations from the CWT assumptions of perfect Gaussian independent distributions for each IS Fourier component. The deviations are more visible at the larger q_x, as $S^{\rm BW}$ moves away from its divergence, and also at larger q_z where the rapid decay of $|\Phi(q_z)|^2 \sim e^{-q_z^2 S(0)}$ in (12) should be balanced (within the CWT assumptions) by the rapid growth of $e^{q_z^2 S(x)}$. Nevertheless, the most useful experimental data should correspond to much lower q_x (that give larger S signal), and for those low q_x values the assumption $S \simeq S^{\rm BW}$ is very accurate.

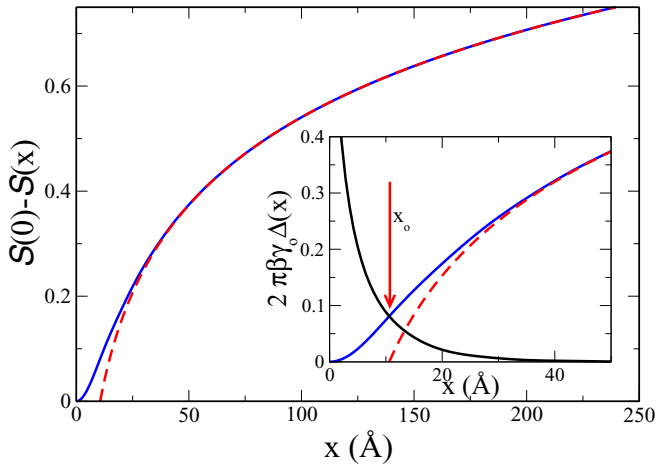

FIG. 5. The height-height correlation function in real space, $\mathcal{S}(0) - \mathcal{S}(x) = \Sigma(x)/(2\pi\beta\gamma_0)$ for tensile stress $P_x = -0.16$ N/m. The full blue line is obtained using Eq. (20), with $\gamma(q_x) = \gamma_0 + \kappa q_x^2$, in a large box with $L = 1$ μm. The dashed red line shows the fit to the shape $\Sigma(x) = \ln(x/x_0)$ in the range where this approximation is valid, $q_u^{-1} \ll x \ll L$. The inset shows (with the same colours) the two curves for low x and their difference (black line) $2\pi\beta\gamma_0\Delta(x)$, with $\Delta(x) \equiv \Sigma(x) - \ln(x/x_0)$. The vertical arrow indicates the x_0 value.

The right column in Fig. 4 explores the dependence with the system size, relevant to compare MD simulations with experiment data, when the surface structure factor $S(q_x, q_z)$ (6) represents the sampling over an area $\sim 1\,\mu\text{m}^2$, much larger than the MD box, and without periodic conditions. The broadening of the density profile $\rho(z)$, and hence the narrowing of $|\Phi(q_z)|$, with increasing $L > L_{\text{MD}}$ should be well described within the CWT assumption (4). Using in (20) the quadratic form $\gamma(q_x) \simeq \gamma_0 + \kappa q_x^2$ we have got $\mathcal{S}(x)$ and $\hat{\mathcal{S}}_n(q_x)$, to obtain $S^{\text{BW}}(q_x, q_z)$ for large (periodic) boxes, up to $L = 32L_{\text{MD}}$ (i.e., about half a micron), well beyond the feasible size of a full MD simulation. Only the $n = 1$ coefficient $\mathcal{S}_n(q_x)$ in (10) remains independent of L, while those for $n \geqslant 2$ grow, reflecting the growth of the maximum $\mathcal{S}(\vec{x})$, at $x = 0$, as $\mathcal{S}(0) = \langle|\xi(\vec{x})|^2\rangle \sim \log(L)/(2\pi\beta\gamma_0)$. The results for $S(q_x, q_z)$ show visible changes when we double the MD size, but a good convergence to a size independent structure factor is obtained for $L > 8L_{\text{MD}}$.

To analyze that large L limit, the factor $e^{q_z^2\mathcal{S}(x)}$ in (12) may be written as $e^{q_z^2\mathcal{S}(0)}e^{-\eta\Sigma(x)}$, with the function $\Sigma(x) \equiv 2\pi\beta\gamma_0(\mathcal{S}(0) - \mathcal{S}(x))$, as used in Fig. 5 over the range ($x \ll L$) in which it depends only on the radial distance $x = |\vec{x}|$ and it is independent of the system size. The size effects and the periodic boundary conditions the simulation box appear only for $x \lesssim L$, as a flattening from the CWT prediction $\Sigma(x) = \ln(x/x_0)$, due to the periodic boundaries.

The constant x_0 depends on $\gamma(q_x)/\gamma_0$ and on the upper cutoff q_u. If the bending constant is large ($q_\kappa \equiv \sqrt{\gamma_0/\kappa} \ll q_u$) the cutoff q_u becomes irrelevant and we get $x_0 = 2e^{-\Gamma_{\text{E}}}/q_\kappa \simeq 1.123\sqrt{\kappa/\gamma_0}$, where Γ_{E} is the Euler's constant. With out lower tensile stress we have $q_\kappa = 0.102$ Å^{-1}, well below q_u but not as much as to make the latter fully irrelevant, and our numerical result $x_0 = 11.33$ Å is close, but not exactly equal, to the theoretical prediction (11.01 Å) for $q_\kappa \ll q_u$. With the tenser graphene sheet we get $x_0 = 4.13$ Å, which reflect more the cutoff q_u than the larger $q_\kappa = 0.356$ Å^{-1}. Therefore the two values of the tensile stress presented here cover the physical distinction between the sharp atomic band-top (represented by q_u) and the gradual increase of $\gamma(q_x)$ (represented by q_κ) as the relevant aspects that control the shape of $\Sigma(x)$ at short distance.

Since $|\Phi(q_z)|^2 e^{q_z^2\mathcal{S}(x)} = |\Phi^{\text{in}}(q_z)|^2 e^{-\eta\Sigma(x)}$, in terms of the ($L$ independent) intrinsic density profile, the only dependence with the size (an boundary conditions) of $S^{\text{BW}}(q_x, q_z)$ comes from the (large) values of $\Sigma(x)$ for large x, near the integration limit. For large L, the factor $e^{-\eta\Sigma(x)}$ is very small on that region and the structure factor should converge to a large L limit, independent of the boundary conditions,

$$S^{\text{BW}}(q_x, q_z) = \frac{|\Phi^{\text{in}}(q_z)|^2}{\beta\gamma_0}\int_0^\infty dx \frac{e^{-\eta\Sigma(x)} - 1}{\eta} J_0(q_x x), \tag{21}$$

where we have to assume that the upper limit for $x = |\vec{x}|$, at some very large value $x \gg x_0$ and $q_x x \gg 1$, is smoothed to avoid the oscillatory effects from the Bessel function $J_0(q_x x)$. That should give a fair representation for the experimental sampling over the coherence section of a x-ray beam and in the left column of Fig. 4 we show that it is very close to the result in large periodic boxes.

Notice that when BW series is approximated by $S^{\text{W}}(q_x, q_z)$, the only dependence with L comes in $|\Phi(q_z)|^2$, with the mean density profile. As $\rho(z)$ becomes broader, with increasing L, Wertheim's prediction $S^{\text{W}}(q_x, q_z)$ becomes lower, particularly at large q_z, making clear that it is not a good representation of the structure factor in a large system. The $\eta = 0$ limit of (21) gives a size independent version of Wertheim's term, with the intrinsic $|\Phi^{\text{in}}(q_z)|$ instead of that with the mean density profile (11). In a liquid-vapour surface, the limit $q_z = 0$ reconciles these two versions of Wertheim's prediction, since $|\Phi^{\text{in}}(0)| = |\Phi(0)| = \Delta\rho$, but for graphene or any other 2D structure, the limit $q_z = 0$ is useless.

For any $\eta = q_z^2/(2\pi\beta\gamma_0) < 2$, the evaluation of (21) may be split as $S^{\text{BW}} = S_0 + S_\Delta$, where

$$S_0(q_x, q_z) = \frac{4\pi|\Phi^{\text{in}}(q_z)|^2}{q_x^2\, q_z^2} \frac{\Gamma(1 - \eta/2)}{\Gamma(\eta/2)} \left(\frac{x_0 q_x}{2}\right)^\eta. \tag{22}$$

in terms of the gamma function Γ, was obtained by Sinha [5,42] assuming that the asymptotic form $\Sigma(x) = \ln(x/x_0)$ may be used over the full range $0 \leqslant x$ in (21), so that $e^{-q_z(S(0)-S(x))} = (x_0/x)^\eta$. This is the usual starting point for the interpretation of surface diffraction data, and we use here the subindex in S_0 to indicate that it depends only on γ_0 [through $\eta = q_z^2/(2\pi\beta\gamma_0)$] and on x_0, as the only relevant measures of the short-range behavior of $\mathcal{S}(x)$. As far as $\eta < 2$, S_0 should be the most important contribution to S^{BW} at low q_x, as shown in Figs. 6 and 7.

Figure 6 presents the results for S^{BW} (full lines) and S_0 (straight dotted lines), for several (small) values of η, as functions of q_x. Since q_z is fixed by the experimental angle of incidence, the $2 - \eta$ slope of the $\ln(S) - \ln(q_x)$ should represent the structure factor at low q_x, when the short-ranged function $\Delta(x)$ contributes very little and $S^{\text{BW}} \simeq S_0$. Then, those straight lines should give direct access to $\beta\gamma_0 =$

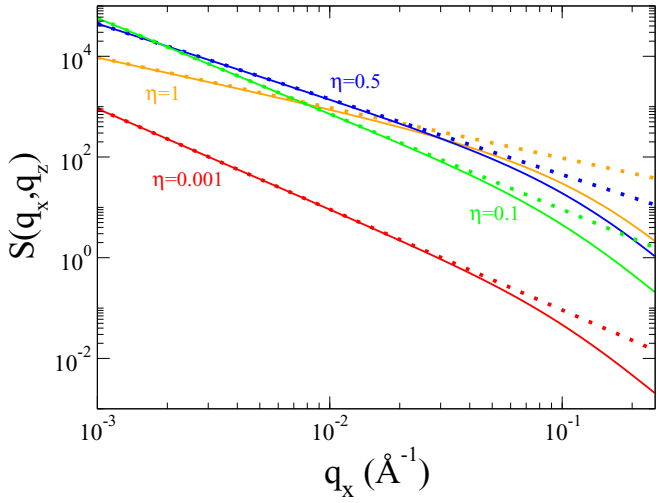

FIG. 6. The structure factor $S(q_z, q_x)$ for our suspended graphene model with tensile stress $P_x = -0.16$ N/m. Full lines: from Eq. (21). Dotted lines: $S_0(q_x, q_z)$ given by Eq. (22). The results are given for several incident angles that fix q_z and $\eta = q_z^2/(2\pi\beta\gamma_0)$.

$q_z^2/(2\pi\eta)$ from the diffuse scattering at very small deviations from the specular reflection (i.e., at low q_x). That may be particularly relevant for suspended graphene sheets, since a direct macroscopic measure of their surface tension may not be available.

In a liquid surface, the maximum scattering signal is obtained at the closest practical approach to the perfect grazing incidence $q_z = \eta = 0$. For graphene, the maximum structure factor appears for $0.1 \lesssim \eta \lesssim 0.5$, depending on the value of

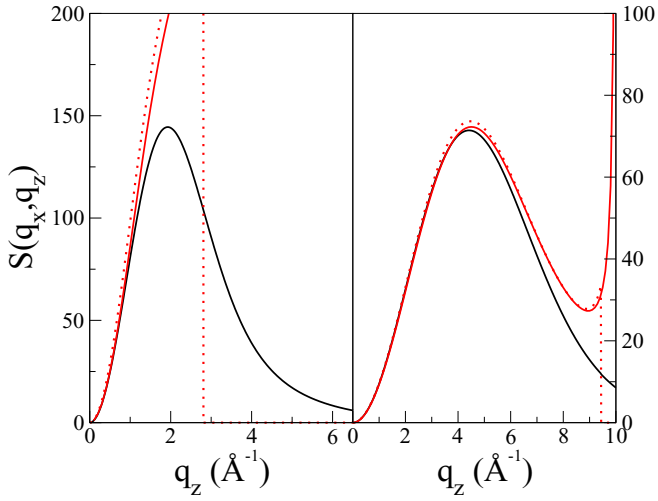

FIG. 7. The black full lines are the results for $S^{\rm BW} = S_0 + S_\Delta$, Eqs. (21)–(23), for the systems with low ($P_{xy} = -0.16$ N/m, left) and high ($P_{xy} = -3.2$ N/m, right) tensile stress. The red dotted lines are Sinha's S_0 asymptotic form, Eq. (22), which may only be calculated for $\eta = q_z^2/(2\pi\beta\gamma_0) < 2$. The full red lines are the usual local approximation $S_{\rm loc}(q_x, q_z)$, Eq. (24), in terms of a $\eta(q_x) = q_z^2/(2\pi\beta\gamma(q_x))$ used in S_0. The range of validity the local approximation is restricted by the poles of $\Gamma(1-\eta(q_x)/2)$, which move to larger q_z as the surface tension γ_0 increases.

q_x. In practice, it would be difficult to extract the value of x_0 from the experimental results for $S \approx S_0$ at very low q_x, since it is entangled with the value of $\Phi^{\rm in}(q_z)$, which may depend on how the graphene sheet is suspended. Any information on κ, and in general on $\gamma(q_x)/\gamma_0$, has to be searched in the deviation between the $S^{\rm BW}(\simeq S)$ and S_0 lines, around $q_x \sim 0.1$ Å^{-1} in Fig. 6.

We find the generic relation

$$S_\Delta(q_x, q_z) = \frac{|\Phi^{\rm in}(q_z)|^2 x_0^\eta}{\beta\gamma_0} \int_0^\infty dx \frac{e^{-\eta\Delta(x)} - 1}{\eta\, x^{\eta-1}} J_0(q_x x), \quad (23)$$

between the deviation, $S_\Delta \equiv S^{\rm BW} - S_0$ (expected for large q_x) and the short-ranged core, $\Delta(x) = \Sigma(x) - \ln(x/x_0)$, in the height-height correlation function. If $q_\kappa \ll q_u$, we know the analytic decaying form $\Delta(x) \sim \sqrt{q_\kappa/q_x} e^{-q_x/q_\kappa}$, while in the opossite case ($q_\kappa > q_u$, as in our tenser system) $\Delta(x)$ has oscillatory decay. In any case, $\Delta(x)$ is a short-ranged function, with decay length comparable to x_0, which may be numerically calculated from (20), and (always for $\eta < 2$) integrated in (23) with no influence of the system size L.

Any validation of a structural model for graphene, as that used in our MD simulation, with experimental data for the structure factor of a suspended graphene layer should address $S_\Delta(q_x, q_z)$. This function contains the dependence with the atomic force field in the model and (in the mesoscopic CWT description) the dependence with κ and q_u, that reflect the atomic interactions in the energy cost to corrugate the layer. Sinha's [5,42] S_0 is the main contribution to S for $q_x \lesssim 0.1$ Å^{-1}, it depends on the macroscopic γ_0 imposed to the suspended layer (both in the MD simulation and in the experimental set up), but it does not reflect the details of the atomic interactions, and cannot provide a validation of the model.

The interpretation of x-ray surface scattering in liquid surfaces [13,23], beyonds Sinha's term (22), used an effective local relationship between $S(q_x, q_z)$ and $\gamma(q_x)$

$$S_{\rm loc}(q_x, q_z) \equiv S_o(q_x, q_z; \eta(q_x)) \equiv \frac{4\pi|\Phi^{\rm in}(q_z)|^2}{q_x^2\, q_z^2} \frac{\Gamma(1-\eta(q_x)/2)}{\Gamma(\eta(q_x)/2)} \left(\frac{x_0 q_x}{2}\right)^{\eta(q_x)}, \quad (24)$$

where the dependence (22) of the asymptotic contribution S_0 with $\eta = q_z^2/(2\pi\beta\gamma_0)$ is changed into the same dependence with $\eta(q_x) = q_z^2/(2\pi\gamma(q_x))$, to describe the full structure factor $S_0 + S_\Delta$. As shown in Fig. 7, this local approximation works rather well for low q_z, but it breaks down as we approach the pole of $\Gamma(1-\eta/2)$ at $\eta(q_x) = 2$. In our system with the lower tensile stress, the range of validity falls short of the maximum $S(q_x, q_z)$, so that the strongest signal of the structure factor could not be analysed within this simple q_x-local assumption. For our system with the higher tensile stress the validity of (24) covers a much larger range of q_x, including the maximum, but it is also much closer to the plain asymptotic assumption $S \simeq S_0$. There has been some discussion [42] on whether the mean or the intrinsic density profile should be used in Sinha's (22) and by extension in (24). The comparison with our results for $S^{\rm BW} = S_0 + S_\Delta$ makes clear that the intrinsic profile is the correct choice; it makes

the structure factor independent of the sampled area and it extends the accuracy of the local approximation as much as possible, for $q_z > 0$.

Depending on the experimental technique used to sample $S(q_x, q_z)$, larger values of q_z might be accessible and, for suspended graphene with low γ_0, the optimal range of observation may shift to $\eta > 2$. In that case the divergence at low q_x disappears, and both Sinha's S_0 and the empirical local description (24) become useless, but still the corrugations of the surface create density correlations that are well described by $S^{\rm BW}$ in (21) and carry information on $\gamma(q_x)$.

VI. THE WAVE-VECTOR-DEPENDENT SURFACE TENSION

We turn now to question how $\gamma(q_x)$ can be obtained from the density correlations. In computer simulations (and in density functional theories), the full access to $G(z_1, z_2, q_x)$ makes the task simpler. In a recent work [39], the problem was addressed for simple and cold liquid surfaces. A main difficulty was to subtract the background G_b of density correlations not associated to the IS fluctuations. That problem was solved through the access (in computer simulations) to the *intrinsic pair correlation*, as explained above. We have seen here that for graphene $G_b \ll G$, and the correlation background may be ignored. The second difficulty, which is shared (and even stronger) for graphene, is the fact that Wertheim's term (5) cannot be taken as a good approximation to the full BW series. If Wertheim's ($n = 1$) term (5) were the main contribution to $\Delta G = G^{\rm BW}$, then the derivative of the density profile, $\rho'(z)$, would be the eigenfunction of $G^{\rm BW}$ with a divergently large eigenvalue as $q_x \to 0$. Therefore it was proposed [20,21] to define a *normal mode* (NM) surface tension

$$\beta\gamma_{\rm NM}(q_x) = \frac{\langle\rho'|\rho'\rangle}{q_x^2\,\langle\rho'|G|\rho'\rangle}, \tag{25}$$

in the usual bra-ket notation

$$\langle\rho'|G|\rho'\rangle = \int dz_1 dz_2\ \rho'(z_1) G(z_1, z_2, q_x)\rho'(z_2) \tag{26}$$

and

$$\langle\rho'|\rho'\rangle = \int dz \rho'(z)^2. \tag{27}$$

This NM assumption appeared to be well founded in the MD-ISM analysis of a Lennard-Jones (LJ) liquid surface, with a typical size for the MD simulation box [43]. However, both for cold liquids (with structured density profiles, in the same simulation box size) or for LJ in a much larger surface size, it was later found [39] that the contributions of the $n \geqslant 2$ terms in the BW series become important. In that case, it is only through the *deconstruction* (dc) of the BW series that the true $\gamma(q_x)$ may be obtained, in terms of the matrices $A_{n,m} = \langle(d^n\rho/dz^n)|(d^m\rho/dz^m)\rangle$ and $B_{n,m}(q_x) = \langle(d^n\rho/dz^n)|G|(d^m\rho/dz^m)\rangle$ over the nonorthogonal basis of the higher order derivatives of the density profile that appear in the BW series. The procedure and its convergence is presented as Ref. [41]. In Fig. 8, we present $\beta\gamma_{\rm dc}(q_x) = [q_x^2 C_{1,1}]^{-1}$ for graphene, calculated from the first diagonal element of the matrix $C = A^{-1}BA^{-1}$, when we use rank 20 matrices to cover

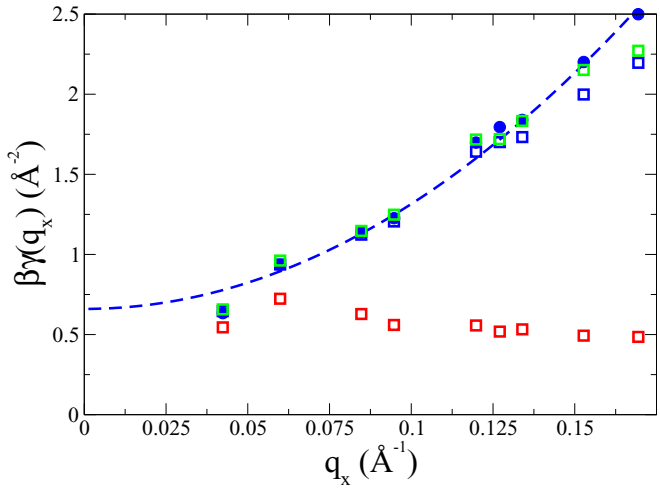

FIG. 8. The wave-vector-dependent surface tension $\gamma(q_x)$ for tensile stress $P_x = -0.16$ N/m. Blue full circles: $\gamma(qx)$ from the fluctuations of the intrinsic surface (3). Dashed blue line the quadratic fit $\gamma(q_x) \simeq \gamma_0 + \kappa q_x^2$ to the blue full circles. Blue empty squares: $\gamma_{\rm dc}(q_x) = [q_x^2 C_{1,1}]^{-1}$ from *deconstruction* (dc) of simulation $G(z_1, z_2, q_x)$. Red empty squares: normal mode result (25), based on Wertheim's correlation term (5). Green squares: $\gamma(q_x)$ from the local relation (24) between the simulation $S(q_x, q_z)$ and $\gamma(q_x)$, as used on the interpretations of x-ray surface scattering in liquid surfaces.

the practical convergence of the BW series. The agreement with the direct ISM $\gamma(q_x)$ is excellent, while the NM version (which corresponds to neglect any $B_{n,m}$ for $n, m > 1$) fails completely.

Recovering $\gamma(q_x)$ from the experimentally accessible $S(q_x, q_z)$ could be more difficult than from the function $G(z_1, z_2; q_x)$ got from computer simulations. The dependence on z_1 and z_2 is partially lost, since the inverse Fourier transform with respect to q_z would give only the dependence on $z_1 - z_2$.

The interpretations of x-ray surface scattering in liquid surfaces [13,23] have been made with the local version (24), solving

$$S(q_x, q_z) = S_{\rm loc}(q_x, q_z) \equiv S_o(q_x, q_z; \eta(q_x)) \tag{28}$$

as an equation for $\eta(q_x)$ with the experimental S. In Fig. 8, we include the result of this hypothesis when we use our MD simulation data for $S(q_x, q_z)$ to represent the experimental structure factor of graphene, that could be obtained from any surface diffraction experiment. The proximity of the $S_0(q_x, q_z)$ and $S_{\rm loc}(q_x, q_z)$ lines in Fig. 7 implies that any noise in $S(q_x, q_z)$ could be strongly amplified in the results for $\eta(q_x)$ and $\gamma(q_x)$. Nevertheless, we found that (28) gives a very accurate result for $\gamma(q_x)$ over the full range $q_x \leqslant 0.2$ Å^{-1}, as far as we keep the incident angle (i.e., the value of q_z) low enough to get $\eta = q_z^2/(2\pi\beta\gamma_0) \lesssim 0.4$. That restriction would not be a practical impediment for large tensile stress. However, in loosely suspended graphene sheets with very small γ_0, the simple "local" interpretation would only be valid for those q_z that give a weak signal, and most of it comes directly from $S_0(q_x, q_z)$. The interpretation of the results for larger values of $S(q_x, q_z)$, when the difference $S_\Delta = S - S_0$

becomes important, may be beyond the range of the local approximation (24) and could require the full (nonlocal) theory of Bedeaux and Weeks, with the generic expression (21).

VII. DISCUSSION

We have presented MD simulations for a realistic model of suspended graphene, to analyze its density correlation function $G(z_1, z_2, q_x)$ and the structure factor $S(q_x, q_z)$. The later could be experimentally accessible from different diffraction techniques (x rays, neutrons, electrons or atomic beams), each with its own (atomic or nuclear) form factor, and with different constrains in the accessible values of q_x and q_z, which we do not discuss here. Our goal is to explore how the common surface structure factor could be used to measure the corrugations of the graphene sheet and how it should be compared with the results of computer simulations for models of that system, that make accessible more information than the experiments.

Along our simulations we got directly $S(q_x, q_z)$ and analysed the thermal fluctuations of the graphene in the theoretical framework of the capillary wave theory (CWT), developed for liquid surfaces. This continuous description for the transverse acoustic band of lattice vibrations is made through a surface Hamiltonian, with a wave-vector -dependent surface tension $\gamma(q_x) = \gamma_0 + \kappa q_x^2$, and we show (see Fig. 1) that it is very accurate up to $q_x \leqslant q_u \approx 0.2$ Å^{-1}. The CWT allows the analysis of the long-ranged correlations developed by the large mean square amplitude of the corrugations with low q_x. Our results prove that suspended graphene is a most promising system to get experimental access to the function $\gamma(q_x)$ from experimental results for $S(q_x, q_z)$. Contrary to the case of liquid surfaces, which have a large correlation background from compressibility (bulklike) fluctuations, graphene is the closest realization of a pure interface. We show here that nearly all the density correlation structure $G(z_1, z_2, q_x)$ obtained in our MD simulation may be very well reproduced (see Figs. 2 and 3) by the theoretical prediction of Bedeaux and Weeks (BW), within the CWT, in terms of a series (8) to include the full effects of the intrinsic surface corrugations, i.e., the Debye-Waller factor of the fluctuating surface [5]. Since the function $\gamma(q_x)$ describes these surface fluctuations, we may hope to gain experimental access to it from the structure factor obtained in diffraction experiments. However, that task has been controversial for liquid surfaces, with puzzling and contradictory results for $\gamma(q_x)$, except for its thermodynamic limit $\gamma(0) = \gamma_0$. The analysis for the graphene sheet presented here, and hopefully its experimental verification, may help to validate the interpretation of some x-ray surface diffraction experiments in liquids, although still with the difficulty associated to the need to subtract their correlation background.

It is crucial to consider the theoretical BW prediction for $G(z_1, z_2, q_x)$ as a full series (8), not only as its first term (5) proposed earlier by Wertheim, and which has been extensively used in the interpretation of computer simulations and diffraction experiments, as well as in the theoretical connection between CWT and the density functional formalism. The need to extend the CWT prediction for $G(z_1, z_2, q_x)$ beyond Wertheim's term had been recently pointed out [39] for structured *cold liquid* surfaces, and also for the surface of a simple (Lennard-Jones) liquid if $G(z_1, z_2, q_x)$ sampled over a large area, with linear size in the range of 1 μm typical of the x-ray beam width in diffraction experiments. In the case of suspended graphene, the higher-order terms of the series (up to $n \approx 20$ terms, for practical convergence) become absolutely necessary. Any term beyond $n = 1$ in the BW series is regular in $q_x = 0$ and nonlocal (in Fourier space); i.e., their contributions to $G(z_1, z_2, q_x)$ and $S(q_x, q_z)$, for a given q_x require the full function $\gamma(q_x)$, from the limit $q_x = 2\pi/L$ imposed by the system size to the upper cutoff q_u. The relationship between $S(q_x, q_z)$ and $\gamma(q_x)$ is global and rather convoluted. Nevertheless the simple local approximation (24) could be quite accurate (at low q_z) and could provide a simple practical tool to get $\gamma(q_x)$ from experimental diffraction data. An important result, from our comparison of the exact nonlocal $S^{\rm BW} = S_0 + S_\Delta$ with the approximated local function $S_{\rm loc}$ is that it clarifies the need to use the intrinsic density profile, rather than the mean one $\rho(z)$, to get the factor $|\Phi^{\rm in}|$. Only in the strict grazing scattering condition, $q_z = 0$, we may recover Wertheim's simple relation to get $\gamma(q_x)$ from $S(q_x, q_z)$ in liquid surfaces, because only in that case all the $n \geqslant 2$ terms in BW series vanish, and $\Phi(0) = \Phi^{\rm in} = \Delta\rho$ makes irrelevant the distinction between the mean and the intrinsic density profile.

However, for graphene (or any other fluctuating 2D system like bilayer membranes), the strict grazing limit $q_z = 0$ is useless, because the lack of density contrast between the two sides of the fluctuation surface makes $\Phi(0) = 0$ and cancels any signal of the corrugations in $S(q_x, 0)$. Therefore, for graphene, bilayer membranes and also for liquid surfaces under practical experimental conditions, we have to analyze the diffraction signal for positive (small) values of $\eta = q_z^2/(2\pi\beta\gamma_0)$. The divergence [5] $S(q_x, q_z) \propto 1/q_x^{2-\eta}$ is the clear signal of the surface fluctuations at very low q_x, which has been clearly observed in liquid surfaces [2,3,13,14] and (since q_z is fixed by the experimental set up) it gives direct access to measure γ_0 from the diffuse scattering signal very close to specular reflection. The deviation from the pure $1/q_x^{2-\eta}$ decay (see Fig. 6) is a measure for the difference $\gamma(q_x)/\gamma_0 - 1 \approx (q/q_\kappa)^2 + \ldots$, with $q_\kappa \equiv \sqrt{\gamma_0/\kappa}$, and also for the influence of the upper cutoff q_u.

The simple quadratic form of $\gamma(q_x)$ for suspended graphene, appears over a rather broad range of q_x. From the experimental results for $S(q_x, q_z)$ the value of γ_0 should be accessible from the exponent η at very low q_x, at a given q_z, and the deviation from the straight lines (Fig. 6) in the $\ln(S)$-$\ln(q_x)$ could be fitted with $q_\kappa = \sqrt{\gamma_0/\kappa}$ as single parameter. If a larger γ_0 makes q_κ grow to approach q_u, this upper cutoff for the continuous description of the atomic fluctuations would become relevant, and change the shape of the curves in Fig. 6. Altogether, the analysis of experimental data for the diffuse scattering on a graphene sheet seems to be possible and certainly interesting, both as a direct access to the properties of this 2D material and as the cleanest experimental test for the interpretation of x-ray surface diffraction experiments in liquid surfaces.

ACKNOWLEDGMENTS

We acknowledge the support of the Spanish Secretariat for Research, Development and Innovation (Grants No. FIS2017-86007-C3, No. PGC2018-096955-B-C44, and No. FPU2015/0248) and from the "Maria de Maeztu" Programme for Units of Excellence in R&D (MDM-2014-0377)

[1] S. Dietrich and A. Haase, Phys. Rep. **260**, 1 (1995).
[2] P. S. Pershan, Colloids Surf. A **171**, 149 (2000).
[3] P. S. Pershan, J. Phys. Chem. B **113**, 3639 (2009).
[4] F. Höfling and S. Dietrich, Europhys. Lett. **109**, 46002 (2015).
[5] S. K. Sinha, E. B. Sirota, S. Garoff, and H. B. Stanley, Phys. Rev. B **38**, 2297 (1988).
[6] V. K. Tewary and B. Yang, Phys. Rev. B **79**, 125416 (2009).
[7] B. Yang and V. K. Tewary, Phys. Rev. B **77**, 245442 (2008).
[8] F. P. Buff, R. A. Lovett, and F. H. Stillinger, Phys. Rev. Lett. **15**, 621 (1965).
[9] R. Evans, Adv. Phys. **28**, 143 (1979).
[10] J. K. Percus and G. Williams, in *Fluid Interfacial Phenomena*, edited by C. Croxton (Wiley, New York, 1986), pp. 1–44.
[11] M. S. Wertheim, J. Chem. Phys. **65**, 2377 (1976).
[12] D. Bedeaux and J. Weeks, J. Chem. Phys. **82**, 972 (1985).
[13] S. Mora, J. Daillant, K. R. Mecke, D. Luzet, A. Braslau, M. Alba, and B. Struth, Phys. Rev. Lett. **90**, 216101 (2003).
[14] D. X. Li, B. Yang, B. H. Lin, M. Meron, J. Gebhardt, T. Graber, and S. A. Rice, Phys. Rev. Lett. **92**, 136102 (2004).
[15] F. Sedlmeier, D. Horinek, and R. R. Netz, Phys. Rev. Lett. **103**, 136102 (2009).
[16] E. Chacón and P. Tarazona, J. Phys.: Condens. Matter **17**, S3493 (2005).
[17] M. Napiórkowski and S. Dietrich, Phys. Rev. E **47**, 1836 (1993).
[18] S. Dietrich and M. Napiórkowski, Phys. Rev. A **43**, 1861 (1991).
[19] K. R. Mecke and S. Dietrich, Phys. Rev. E **59**, 6766 (1999).
[20] E. M. Blokhuis, J. Kuipers, and R. L. C. Vink, Phys. Rev. Lett. **101**, 086101 (2008).
[21] E. M. Blokhuis, J. Chem. Phys. **130**, 014706 (2009).
[22] E. Chacón and P. Tarazona, J. Phys.: Conds. Matter **28**, 244014 (2016).
[23] C. Fradin, A. Braslau, D. Luzet, D. Smilgles, M. Alba, N. Boudet, K. Mecke, and J. Daillant, Nature **403**, 871 (2000).
[24] J. H. Los and A. Fasolino, Phys. Rev. B **68**, 024107 (2003).
[25] J. H. Los, L. M. Ghiringhelli, E. J. Meijer, and A. Fasolino, Phys. Rev. B **72**, 214102 (2005).
[26] R. Ramírez, E. Chacón, and C. P. Herrero, Phys. Rev. B **93**, 235419 (2016).
[27] R. Ramírez and C. P. Herrero, Phys. Rev. B **95**, 045423 (2017).
[28] C. P. Herrero and R. Ramírez, J. Chem. Phys. **148**, 102302 (2018).
[29] M. E. Tuckerman, B. J. Berne, and G. J. Martyna, J. Chem. Phys. **97**, 1990 (1992).
[30] G. J. Martyna, A. Hughes, and M. E. Tuckerman, J. Chem. Phys. **110**, 3275 (1999).
[31] M. E. Tuckerman and A. Hughes, in *Classical and Quantum Dynamics in Condensed Phase Simulations*, edited by B. J. Berne, G. Ciccotti, and D. F. Coker (Word Scientific, Singapore, 1998), p. 311.
[32] R. Ramírez and C. P. Herrero, J. Chem. Phys. **149**, 041102 (2018).
[33] R. J. T. Nicholl, N. V. Lavrik, I. Vlassiouk, B. R. Srijanto, and K. I. Bolotoin, Phys. Rev. Lett. **118**, 266101 (2017).
[34] G. J. Martyna, M. E. Tuckerman, D. J. Tobias, and M. L. Klein, Mol. Phys. **87**, 1117 (1996).
[35] E. Chacón and P. Tarazona, Phys. Rev. Lett. **91**, 166103 (2003).
[36] F. Bresme, E. Chacón, and P. Tarazona, Phys. Chem. Chem. Phys. **10**, 4704 (2008).
[37] E. Chacón, E. M. Fernández, D. Duque, R. Delgado-Buscalioni, and P. Tarazona, Phys. Rev. B **80**, 195403 (2009).
[38] R. Delgado-Buscalioni, E. Chacón, and P. Tarazona, Phys. Rev. Lett. **101**, 106102 (2008).
[39] J. Hernández-Muñoz, E. Chacón, and P. Tarazona, J. Chem. Phys. **149**, 124704 (2019).
[40] B. Shevitski, M. Mecklenburg, W. A. Hubbard, E. R. White, B. Dawson, M. S. Lodge, M. Ishigami, and B. C. Regan, Phys. Rev. B **87**, 045417 (2013).
[41] See Supplemental Material at http://link.aps.org/supplemental/10.1103/PhysRevB.100.195424 which includes a study of the convergence of the Bedeaux-Weeks series and of its deconstruction.
[42] H. Tostmann, E. DiMasi, P. S. Pershan, B. M. Ocko, O. G. Shpyrko, and M. Deutsch, Phys. Rev. B **59**, 783 (1999).
[43] J. Hernández-Muñoz, E. Chacón, and P. Tarazona, J. Chem. Phys. **148**, 084702 (2018).